



CHORUS

This is the accepted manuscript made available via CHORUS. The article has been published as:

Ultralow-Frequency Collective Compression Mode and Strong Interlayer Coupling in Multilayer Black Phosphorus

Shan Dong, Anmin Zhang, Kai Liu, Jianting Ji, Y. G. Ye, X. G. Luo, X. H. Chen, Xiaoli Ma, Yinghao Jie, Changfeng Chen, Xiaoqun Wang, and Qingming Zhang

Phys. Rev. Lett. **116**, 087401 — Published 26 February 2016

DOI: [10.1103/PhysRevLett.116.087401](https://doi.org/10.1103/PhysRevLett.116.087401)

Ultralow-frequency collective compression mode and strong interlayer coupling in multilayer black phosphorus

Shan Dong¹, Anmin Zhang¹, Kai Liu¹, Jianting Ji¹, Y. G. Ye², X. G. Luo^{2,6}, X. H. Chen^{2,5,6},
Xiaoli Ma¹, Yinghao Jie¹, Changfeng Chen³, Xiaoqun Wang^{1,4,6}, and Qingming Zhang^{1,6*}

¹ *Department of Physics, Beijing Key Laboratory of Opto-electronic Functional Materials & Micro-nano Devices, Renmin University of China, Beijing 100872, P. R. China*

² *Hefei National Laboratory for Physical Sciences at Microscale and Department of Physics, University of Science and Technology of China and Key Laboratory of Strongly-coupled Quantum Matter Physics, Chinese Academy of Sciences, Hefei, Anhui 230026, P. R. China*

³ *Department of Physics and High Pressure Science and Engineering Center, University of Nevada, Las Vegas, Nevada 89154, USA*

⁴ *Department of Physics and Astronomy, Shanghai Jiao Tong University, Shanghai 200240, P. R. China*

⁵ *High Magnetic Field Laboratory, Chinese Academy of Sciences, Hefei, Anhui 230031, P. R. China*

⁶ *Collaborative Innovation Center of Advanced Microstructures, Nanjing 210093, P. R. China*

(Dated: February 4, 2016)

The recent renaissance of black phosphorus (BP) as a two-dimensional (2D) layered material has generated tremendous interest, but its unique structural characters underlying many of its outstanding properties still need elucidation. Here we report Raman measurements that reveal an ultralow-frequency collective compression mode (CCM) in BP, which is unprecedented among similar 2D layered materials. This novel CCM indicates an unusually strong interlayer coupling, and this result is quantitatively supported by a phonon frequency analysis and first-principles calculations. Moreover, the CCM and another branch of low-frequency Raman modes shift sensitively with changing number of layers, allowing an accurate determination of the thickness up to tens of atomic layers, which is considerably higher than previously achieved by using high-frequency Raman modes. These findings offer fundamental insights and practical tools for further exploration of BP as a highly promising new 2D semiconductor.

PACS numbers: 78.30.-j, 63.22.Np, 63.20.-e

Two-dimensional (2D) layered semiconductor black phosphorus (BP) has received renewed interest recently. Similar to graphene [1] and transition-metal dichalcogenides (TMDs) [2], BP has a corrugated honeycomb lattice [3] with strong intralayer covalent bonding and weak interlayer van der Waals coupling [4], and it has an orthorhombic crystal symmetry D_{2h} with an interlayer distance of $\sim 5.3\text{\AA}$ [5]. BP also possesses widely tunable band gaps of 0.33–2.0 eV from its bulk to few-layer forms [6]. Its room-temperature mobility can reach up to $\sim 1000\text{ cm}^2\text{V}^{-1}\text{s}^{-1}$ with a high on-off ratio [7]. These properties hold promising prospects for electronic and opto-electronic applications [8, 9], and many of them are attributed to BP's unique structural characters that still need further exploration for fundamental understanding of this novel 2D semiconductor [10].

Raman scattering is a versatile technique for investigating fundamental lattice dynamics, electronic and excitonic properties of low-dimensional materials. For layered compounds, there exist two basic modes reflecting relative motions between neighboring layers, i.e., the compression/breathing and shear modes. **These modes offer essential information about the interlayer coupling, which has played important roles in probing the lattice dynamics and electronic properties of few-layer graphene and TMD systems [11–19]. The Raman frequencies shift with the flake thickness, thus allowing an accurate deter-**

mination of the layer number, and such shifts also measure the interlayer electron hopping.

In this Letter, we report observation of novel Raman modes with very low frequencies in multilayer BP. They belong to two distinct branches of compression modes, one with low frequencies that approach 100 cm^{-1} with increasing layer number and the other with ultralow frequencies that approach 10 cm^{-1} . The low-frequency (LF) mode exhibits a clear layer-number dependence described by a linear-chain model. Surprisingly, the ultralow-frequency (ULF) mode scales with the layer number in the limit of large interlayer coupling, suggesting an unusually stronger interlayer coupling in multilayer BP. Our phonon frequency analysis and first-principles calculations provide further evidence of strong interlayer coupling in BP. These scaling results offer a sensitive and robust method for an accurate determination of layer thickness of atomically thin BP films. The unexpectedly strong interlayer coupling in BP imposes important constraints on the modeling and design of BP-based device applications.

The BP flakes with various thicknesses were obtained by mechanical exfoliation from bulk crystals synthesized under high pressure. The freshly exfoliated flakes were quickly transferred to a 300-nm-thick SiO_2 substrate on a Si wafer. The optical microscope and AFM imaging were employed to determine the thickness. Then the

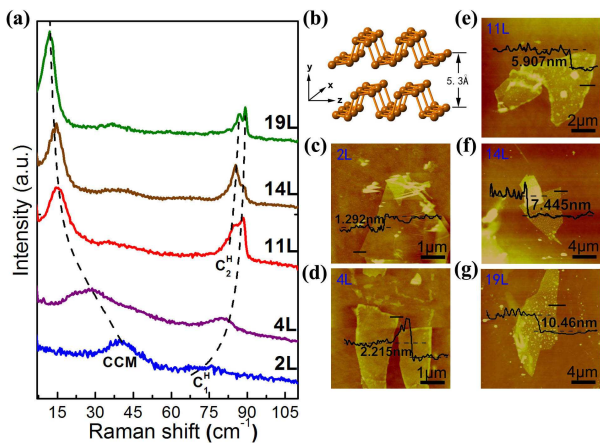


FIG. 1: (color online) (a) Two branches of Raman modes at low (100 cm^{-1}) and ultralow (10 cm^{-1}) frequencies with changing layer number. (b) An illustration of the layered BP structure. (c)-(g) The layer thickness of the selected flakes is accurately characterized by AFM imaging in each case.

flakes were covered with a PMMA protective film for Raman measurements, which were performed with a Jobin Yvon HR800 single-grating-based micro-Raman system equipped with a volume Bragg grating low-wavenumber suite, a liquid-nitrogen cooled back-illuminated CCD detector and a 633 nm laser (Melles Griot). The laser was focused into a spot of $\sim 5 \mu\text{m}$ in diameter on the sample surface, with a power less than $100 \mu\text{W}$. Each spectrum was measured more than three times to check the consistency and any possible effect of the flake size or homogeneity [24]. AFM imaging was carried out with a Nanoscope IIIa Dimension 3100 AFM system (Digital Instruments). First-principles calculations were carried out with the Vienna Ab initio Simulation Package (VASP) [20, 21] with the use of the projector augmented wave method [22, 23]. The computational details are given in Supplemental Material [24].

To establish an accurate relation between the layer number and phonon modes, five BP flakes with different thicknesses were selected for Raman measurements and simultaneous atom force microscopy (AFM) imaging (Fig. 1), which directly gives the thickness of each flake. In the Raman spectra for each flake, two phonon branches, namely the LF and ULF Raman modes, are observed, and they evolve differently with increasing layer number: not only they shift in opposite directions as the layer number increases with the LF mode moving to higher frequencies while the ULF mode moving to lower frequencies, but more importantly they follow qualitatively different scaling behavior (see below for a detailed analysis). Meanwhile, the widths of these modes consistently become narrower with increasing layer number.

The significant changes in both the frequency and width of the LF and ULF Raman modes can serve as a clear and accurate indicator of the layer number in

the BP flakes. To quantify this observation, we have fit the layer-number dependence of the mode frequencies according to a linear-chain model (see details below). For a high-quality fitting, we have made additional Raman measurements on a large amount of BP flakes as shown in Fig. 2(a). The smooth evolutions of both the frequencies and widths of the observed modes allow accurate assignments for all the obtained spectra. Their frequencies follow two well-established fitting curves, thus allowing an accurate determination of the layer number [see Fig. 2(b) and (c)]. We further checked the layer-number dependence of the high-frequency ($\sim 470 \text{ cm}^{-1}$) A_g^2 mode and obtained consistent results [24]. It should be noted that the maximum shift in frequency for the A_g^2 mode is limited to $\sim 3 \text{ cm}^{-1}$ and the mode frequency nearly stops changing in samples with more than five layers [25]. By comparison, the maximum frequency shift in our measurements is as large as 32 cm^{-1} for the ULF mode and 19 cm^{-1} for the LF mode, and the mode positions are still sensitive to the thickness change even beyond several tens of layers. This observation demonstrates that the ULF and LF Raman modes in BP offer a highly effective method to determine the thickness of atomically thin films over a wide range.

The LF and ULF modes, which are absent in both bulk and monolayer cases, are assigned to interlayer modes, as previously observed in h-BN, few-layer graphene and TMD materials [11–19]. But unlike honeycomb-based TMDs and graphene, BP has an orthogonal lattice with point group D_{2h} , which only allows non-degenerate A_g/B_g modes [24]. In other words, the E-symmetry shear modes allowed in TMDs and graphene are symmetry-forbidden in few-layer BP [5, 26, 27]. First-principles calculations and symmetry analysis further demonstrate that both the LF and ULF branches observed in BP come from interlayer compression motions [24].

We first examine the spectra of the ULF mode. Surprisingly, the layer-number dependence of the ULF branch shown in Fig. 2(c) clearly does not follow the derived relation $\omega = \omega_0 \sqrt{(1 - \cos(\pi/N))}$ or $1/N$ from the standard linear-chain model. Instead, it scales as $1/\sqrt{N}$. This scaling behavior is still compatible with the linear-chain model, but only in the limit of large interlayer coupling. In other words, this unusual ULF mode indicates that the interlayer coupling is strong enough to couple all the layers together, resulting in an in-phase compression motion of all the layers in the sample relative to the substrate [30] [Fig. 2(e)]. It can be regarded as a collective motion of a composite object with N times the mass per unit area of one BP layer. A similar mode has been observed in epitaxial KBr film on NaCl substrate [31].

The assignment of the collective compression mode is also supported by polarization measurements. Symmetry analysis and first-principles calculations indicate that the allowed compression modes have A-symmetry, for which one may in principle expect periodic modulations in in-

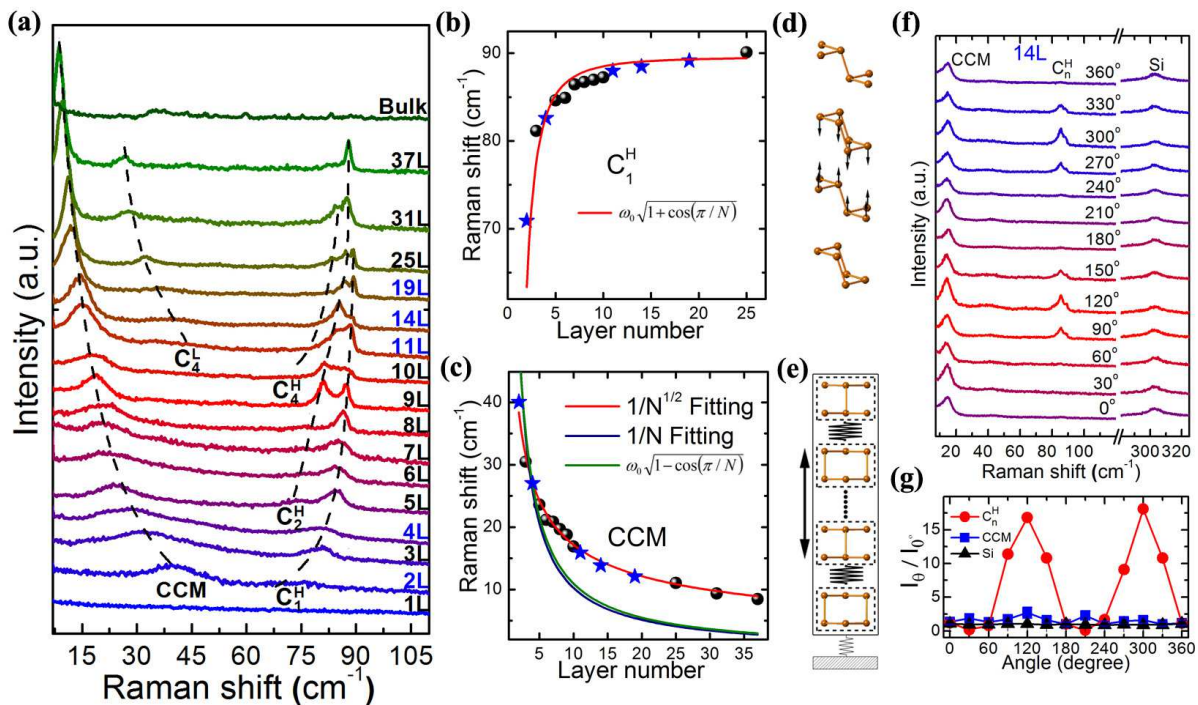


FIG. 2: (color online) (a) Raman spectra collected from few-layer to bulk BP samples. The blue layer number means that the corresponding flake thickness is checked by AFM imaging; CCM and C_n^H/C_n^L denote the collective compression mode, the n th-order compression modes from the higher/lower branch with low/ultralow frequencies, respectively. (b) Layer-number dependence of the C_1^H mode. The corresponding vibration pattern is illustrated in (d). The data are extracted from the Raman spectra in (a), and those represented by solid stars from those marked by blue layer numbers, which are confirmed by AFM imaging. The red solid curve is the linear-chain fitting. (c) Layer-number dependence of the CCM mode. The corresponding vibration pattern is illustrated in (e). The data are obtained in the same way as in (b). The red, blue and green solid curves are the fittings by $1/\sqrt{N}$, $1/N$ and the standard linear-chain model. (f) Polarization measurements of the Raman modes. Both the intensities and frequencies are carefully monitored and calibrated by the second-order silicon mode at 302 cm^{-1} . The angle dependence of the integrated intensities of the observed modes is shown in (g).

tensity by tuning the polarization angle [24]. For the LF branch, the modulations follow the A-symmetry Raman tensors, in agreement with the observations for the high-frequency Raman modes and photoluminescence [32–34]; but for the ULF branch, there is only a weak anisotropy [Fig. 2(f) and (g)]. This contrasting phenomenon stems from the fact that the LF mode comes from the relative vibration between the BP layers while the ULF mode represents a rigid motion of the whole N -layers relative to the substrate. Therefore, the in-plane anisotropy of the ULF mode is significantly weakened due to the smearing of the relatively isotropic substrate, resulting in the observed weak polarization dependence.

As shown in Fig. 2(b), the layer-number dependence of the mode frequencies of the LF branch follows the prediction of a standard linear-chain model, which gives $\omega = \omega_0 \sqrt{1 + \cos(\pi/N)}$, where ω is phonon frequency, N layer number and ω_0 a fitting parameter. The corresponding atomic vibration pattern is illustrated in

Fig. 2(d). The linear-chain model gives [11] $\omega_0 = \frac{1}{\sqrt{2\pi c}} \sqrt{\frac{\alpha}{\mu}}$, where $\omega_0 = 71\text{ cm}^{-1}$ is the frequency of the first-order interlayer compression mode C_1^H in bilayer case [Fig. 2(a)], c the speed of light, $\mu = 1.42 \times 10^{-26}\text{ kg} \cdot \text{\AA}$ the mass per unit cell area. These results lead to an interlayer force constant $\alpha = 1.27 \times 10^{20}\text{ N/m}^3$, which is in good agreement with a recently calculated value [28]. It is noted that this force constant is significantly larger than its counterpart for MoS₂ and graphene [11, 12], which suggests a much stronger interlayer coupling in multi-layer BP (see Table I). This is consistent with the results from the ULF branch (see below). Following $C_{33} = \alpha \cdot t$, where t is the distance between neighboring layers, we obtain the stretching modulus $C_{33} \sim 67.3\text{ GPa}$, which is very close to the value 70.0 GPa measured by neutron scattering and the calculated value 70.8 GPa [27, 29].

Using the general layer-number dependence given by the linear-chain model, $\omega_N = \omega_0 \sqrt{1 \pm \cos(n\pi/N)}$, we can make a comprehensive assignment for the observed

TABLE I: Comparison of the interlayer coupling in BP, MoS₂ and graphene. Here α is the experimental interlayer force constant, K_{intra} (K_{inter}) is the intralayer (interlayer) spring force constant deduced from measured phonon frequencies, E_B is the interlayer binding energy per unit area calculated using three types of van der Waals corrections: (A) Optb88-vdW, (B) DFT-D2, and (C) Optb86-vdW [24].

| | α (10^{18} N/m ³) | K_{intra}/K_{inter} | E_B (meV/Å ²) | | |
|------------------|--|-----------------------|-----------------------------|-----|-----|
| | | | (A) | (B) | (C) |
| BP | 127 ^a | 26 | 31 | 23 | 35 |
| MoS ₂ | 29 ^b | 100 | 26 | 18 | 27 |
| graphene | 12.8 ^c | / | 26 | 21 | 26 |

*a: this work; b: Ref. [12]; c: Ref. [11]

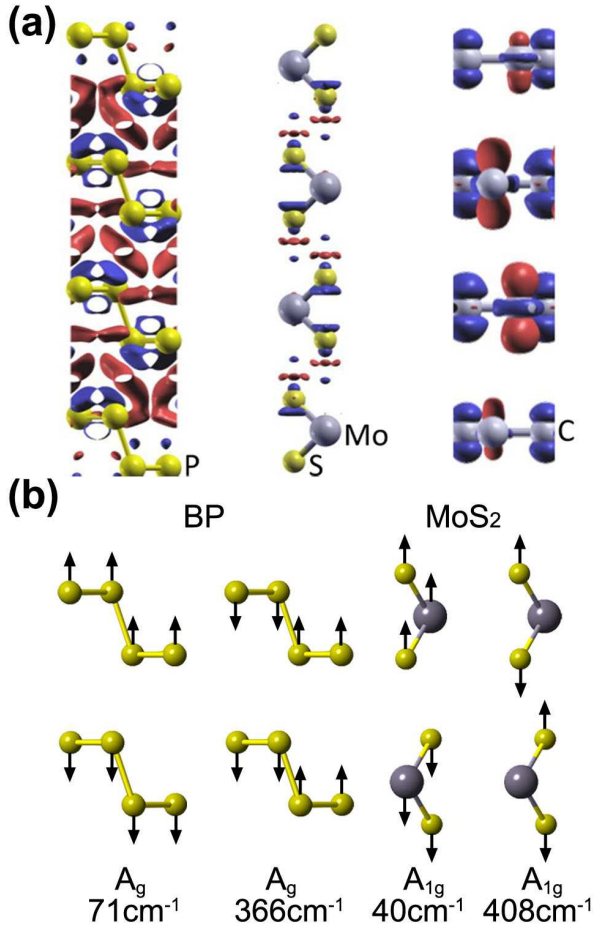


FIG. 3: (color online) (a) Calculated charge difference density profiles for few-layer BP, MoS₂, and graphene. The regions gaining/losing electrons are marked in purple/blue. (b) Displacement patterns and measured frequencies of comparable intra- and inter-layer compression modes in BP (left) and MoS₂ (right).

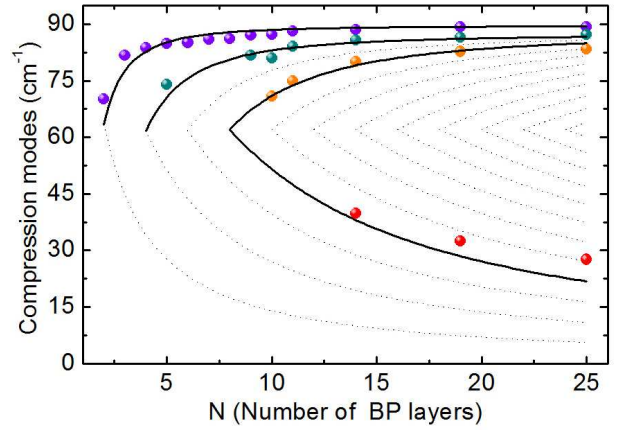


FIG. 4: (color online) Assignment of the observed compression modes by fan diagram. The solid and dashed lines are produced by the linear-chain model. The circles are the positions of the observed compression modes in Fig. 2(a) except for the CCM.

compression modes except for the CCM mode. These assigned modes follow the fan diagrams (Fig. 4), similar to the case in MoS₂ [13].

The strong interlayer coupling revealed by the $1/\sqrt{N}$ scaling behavior can be quantitatively estimated by a phonon frequency analysis. The frequency ratio of inter- and intra-layer modes with comparable vibration patterns offers a good measure of relative interlayer coupling, since $\omega^2 \propto K/m$ in a simplified spring model, where K is the spring force constant. Based on the data for the intra- and inter-layer shear modes, the intra-layer spring constant is estimated to be 100 times larger than the inter-layer one in MoS₂ [35]. Using the intra- ($A_{1g} \sim 40$ cm⁻¹) and inter-layer ($A_{1g} \sim 408$ cm⁻¹) compression modes in MoS₂ [Fig. 3(b)], a similar ratio was obtained.[12, 13] Following this established procedure, we have identified [Fig. 3(b)] the C_1^H (71 cm⁻¹, A_g) mode as the corresponding interlayer version of the high-frequency intra-layer A_g mode (366 cm⁻¹). We therefore obtain a ratio of ~ 26 between the intra- and inter-layer spring force constants in BP, which is much smaller than that in MoS₂.

We further made first-principles calculations to examine the interlayer coupling. In Fig. 3(a), the charge difference density profiles are shown for few-layer BP, MoS₂, and graphene. More significant charge redistributions can be clearly seen in few-layer BP, which indicates stronger overlapping of the interlayer orbitals. The calculated results on the interlayer binding energy per unit area, E_B (Table I), also quantitatively support that BP has the strongest interlayer coupling. It has been suggested that the strong interlayer coupling in BP stems from the electronic hybridization of the lone electron pairs beyond the van der Waals epitaxy [28].

In summary, we have successfully observed low-frequency interlayer compression modes in BP films over

a wide range of thickness from a few layers to tens of layers. The sensitive layer-number dependence of the frequency shift of these modes enables an accurate determination of the number of atomic layers in multilayer BP. A low-frequency branch of the interlayer modes can be well described by a linear-chain model, which has been used to describe few-layer MoS₂ and graphene. In addition, we observed a novel ultralow-frequency collective compression mode that scales with layer number N as $1/\sqrt{N}$, which is a clear indication of an unusually strong interlayer coupling. This surprising result, which is unprecedented in similar 2D layered materials, is further supported by first-principles calculations and a phonon frequency analysis. The obtained ratio of ~ 26 for the intra- and inter-layer force constant in BP is a factor of four smaller than that in MoS₂. This strong interlayer coupling has significant implications for understanding and modeling of the electronic and mechanical properties crucial to applications of BP-based nanodevices.

This work was supported by the Ministry of Science and Technology of China (973 projects: 2012CB921701 and 2012CB921704) and the NSF of China. Q.M.Z. and K. L. was supported by the Fundamental Research Funds for the Central Universities, and the Research Funds of Renmin University of China (10XNI038, 14XNLQ03). Computational resources have been provided by the PLHPC at RUC. The atomic structures were prepared with the XCRYSDEN program [36].

* Electronic address: qmzhang@ruc.edu.cn

- [1] A. H. Castro Neto, F. Guinea, N. M. R. Peres, K. S. Novoselov and A. K. Geim, *Rev. Mod. Phys.* **81**, 109 (2009).
- [2] A. B. Kaul, *J. Mater. Res.* **29**, 348 (2014).
- [3] A. Brown and S. Rundqvist, *Acta Crystallogr.* **19**, 684 (1965).
- [4] A. S. Rodin, A. Carvalho and A. H. Castro Neto, *Phys. Rev. Lett.* **112**, 176801 (2014).
- [5] X. Ling, L. B. Liang, S. X. Huang, A. A. Puretzky, D. B. Geohegan, B. G. Sumpter, J. Kong, V. Meunier and M. S. Dresselhaus, *Nano Lett.* **15**, 4080 (2015).
- [6] V. Tran, R. Soklaski, Y. F. Liang and L. Yang, *Phys. Rev. B* **89**, 235319 (2014).
- [7] L. K. Li, Y. J. Yu, G. J. Ye, Q. Q. Ge, X. D. Ou, H. Wu, D. L. Feng, X. H. Chen and Y. B. Zhang, *Nat. Nanotechnol.* **9**, 372 (2014).
- [8] M. Buscema, D. J. Groenendijk, S. I. Blanter, G. A. Steele, H. S. J. van der Zant and A. Castellanos-Gomez, *Nano Lett.* **14**, 3347 (2014).
- [9] R. Fei and L. Yang, *Nano Lett.* **14**, 2884 (2014).
- [10] L. Kou, C. F. Chen, and S. C. Smith, *J. Phys. Chem. Lett.* **6**, 2794 (2015).
- [11] P. H. Tan, W. P. Han, W. J. Zhao, Z. H. Wu, K. Chang, H. Wang, Y. F. Wang, N. Bonini, N. Marzari, N. Pugno, G. Savini, A. Lombardo and A. C. Ferrari, *Nat. Mater.* **11**, 294 (2012).
- [12] H. L. Zeng, B. R. Zhu, K. Liu, J. H. Fan, X. D. Cui and Q. M. Zhang, *Phys. Rev. B* **86**, 241301 (2012).
- [13] X. Zhang, W. P. Han, J. B. Wu, S. Milana, Y. Lu, Q. Q. Li, A. C. Ferrari and P. H. Tan, *Phys. Rev. B* **87**, 115413 (2013).
- [14] X. Lu, M. Iqbal Bakti Utama, J. H. Lin, X. Luo, Y. Y. Zhao, J. Zhang, S. T. Pantelides, W. Zhou, S. Y. Quek and Q. H. Xiong, *Adv. Mater.* **27**, 4502 (2015).
- [15] M. O'Brien, N. McEvoy, D. Hanlon, K. Lee, R. Gatenby, J. N. Coleman and G. S. Duesberg, *Phys. Status Solidi B* **252**, 2385 (2015).
- [16] Y. Y. Zhao, X. Luo, H. Li, J. Zhang, P. T. Araujo, C. K. Gan, J. Wu, H. Zhang, S. Y. Quek, M. S. Dresselhaus, and Q. H. Xiong, *Nano Lett.* **13**, 1007 (2013).
- [17] S. Y. Chen, C. X. Zheng, M. S. Fuhrer and J. Yan, *Nano Lett.* **15**, 2526 (2015).
- [18] G. Froehlicher, E. Lorchat, F. Fernique, C. Joshi, A. Molina-Sánchez, L. Wirtz and S. Berciaud, *Nano Lett.* **15**, 6481 (2015).
- [19] X. X. Xi, L. Zhao, Z. F. Wang, H. Berger, L. Forró, J. Shan and K. F. Mak, *Nat. Nanotechnol.* **10**, 765 (2015).
- [20] G. Kresse and J. Hafner, *Phys. Rev. B* **47**, 558 (1993).
- [21] G. Kresse and J. Furthmüller, *Phys. Rev. B* **54**, 11169 (1996).
- [22] P. E. Blöchl, *Phys. Rev. B* **50**, 17953 (1994).
- [23] G. Kresse and D. Joubert, *Phys. Rev. B* **59**, 1758 (1999).
- [24] See Supplemental Material, which includes Refs. [37]-[42], for details on the confirmation of the layer number assignment by the high-frequency A_g^2 mode, a comparison of the Raman tensors of the interlayer modes in bilayer MX₂, graphene and BP, calculated low-frequency optical modes in few-layer BP, the Raman spectra of the BP flakes with/without PMMA glue covering, effects of the flake size on Raman spectra, an assessment of the leakage of the infrared B_{1u} mode, and the first-principles calculations.
- [25] W. L. Lu, H. Y. Nan, J. H. Hong, Y. M. Chen, C. Zhu, Z. Liang, X. Y. Ma, Z. H. Ni, C. H. Jin and Ze Zhang, *Nano Res.* **7**, 853 (2014).
- [26] J. W. Jiang, B. S. Wang and H. S. Park, arXiv:1412.7587 (2014).
- [27] Y. Q. Cai, Q. Q. Ke, G. Zhang, Y. P. Feng, V. B. Shenoy and Y. W. Zhang, *Adv. Funct. Mater.* **25**, 2230 (2015).
- [28] Z. X. Hu, X. H. Kong, J. S. Qiao, B. Normand and W. Ji, arXiv:1503.06735 (2015).
- [29] A. Yoshihara, T. Fujimura, Y. Oka, H. Fujisaki and I. Shirovani, *J. Phys. Soc. Jpn* **56**, 1223 (1987).
- [30] N. S. Luo, P. Ruggerone and J. P. Toennies, *Phys. Rev. B* **54**, 5051 (1996).
- [31] S. A. Safron, G. G. Bishop, J. Duan, E. S. Gillman, J. C. Skofronick, N. S. Luo and P. Ruggerone, *J. Phys. Chem.* **97**, 2270 (1993).
- [32] J. X. Wu, N. N. Mao, L. M. Xie, H. Xu and J. Zhang, *Angew. Chem.* **127**, 2396 (2015).
- [33] S. Zhang, J. Yang, R. J. Xu, F. Wang, W. F. Li, M. Ghufuran, Y. W. Zhang, Z. F. Yu, G. Zhang, Q. H. Qin and Y. R. Lu, *ACS Nano* **8**, 9590 (2014).
- [34] X. M. Wang, A. M. Jones, K. L. Seyler, V. Tran, Y. Jia, H. Zhao, H. Wang, L. Yang, X. D. Xu and F. N. Xia, *Nat. Nanotechnol.* **10**, 517 (2015).
- [35] J. L. Verble, T. J. Wietling and P. R. Reed, *Solid State Commun.* **11**, 941 (1972).
- [36] A. Kokalj, *Comp. Mater. Sci.* **28**, 155 (2003).
- [37] A. Favron, E. Gaufrés, F. Fossard, P. L. Lévesque,

- A-L. Phaneuf-L'Heureux, N. Y-W. Tang, A. Loiseau, R. Leonelli, S. Francoeur, R. Martel, Preprint at <http://arXiv.org/abs/1408.0345> (2014).
- [38] S. Sugai, S. and I. Shirovani, Solid state Commun. **53**, 753 (1985).
- [39] J. P. Perdew, K. Burke, and M. Ernzerhof, Phys. Rev. Lett. **77**, 3865 (1996).
- [40] S. Grimme, J. Comput. Chem. **27**, 1787 (2006).
- [41] J. Klimés, D. R. Bowler, and A. Michaelides, Phys. Rev. B **83**, 195131 (2011).
- [42] T. Björkman, A. Gulans, A. V. Krasheninnikov, and R. M. Nieminen, Phys. Rev. Lett. **108**, 235502 (2012).